

Article

Analysis of Vibration Responses Induced by Metro Operations Using a Probabilistic Method

Zongzhen Wu ¹, Chunyang Li ^{1,*}, Weifeng Liu ² , Donghai Li ², Wenbin Wang ¹ and Bin Zhu ¹

¹ Urban Rail Transit Centre, China Academy of Railway Sciences Corporation Limited, Beijing 100081, China; wzzlogos@hotmail.com (Z.W.); 13811667172@126.com (W.W.); 15682538713@163.com (B.Z.)

² Key Laboratory of Urban Underground Engineering of Ministry of Education, Beijing Jiaotong University, Beijing 100044, China; wfliu@bjtu.edu.cn (W.L.); 22110330@bjtu.edu.cn (D.L.)

* Correspondence: lycars@163.com

Abstract: The environmental vibrations of tunnels and soil caused by metro operations is one of the most important issues in the field of environmental geotechnical engineering. Recent studies in metro-induced vibrations have revealed significant uncertainties in the vibration responses of tunnels and the surrounding soil. A two-step method of obtaining train loads considering uncertainty was introduced. The first step was to obtain the train loads via an inverse model based on measurements, and the second step was to quantify the uncertainty of train loads based on complex principal component analysis. A portion of a tunnel of the Beijing metro was selected as the object of study, where the vertical accelerations on the rail and on the tunnel wall were measured under different train speeds of 35, 45 and 55 km/h. Inputting the train loads based on the measured rail accelerations into an axisymmetric numerical model, established using ANSYS, the vibration responses of the tunnel wall in a probabilistic framework were calculated and were compared with the measured results. By using an accuracy index that considers both calculation bias and uncertainty, the accuracy of the calculated vibration response was quantitatively evaluated. It can be concluded that the calculated vibration response can reflect the actual vibration level and uncertainty of the tunnel wall. The accuracies of the calculated results under different speeds were generally high while showing a slight difference in amplitude.



Citation: Wu, Z.; Li, C.; Liu, W.; Li, D.; Wang, W.; Zhu, B. Analysis of Vibration Responses Induced by Metro Operations Using a Probabilistic Method. *Symmetry* **2024**, *16*, 145. <https://doi.org/10.3390/sym16020145>

Academic Editors: Yao Bai, Renliang Shan and Victor A. Eremeyev

Received: 3 December 2023

Revised: 17 January 2024

Accepted: 22 January 2024

Published: 26 January 2024



Copyright: © 2024 by the authors. Licensee MDPI, Basel, Switzerland. This article is an open access article distributed under the terms and conditions of the Creative Commons Attribution (CC BY) license (<https://creativecommons.org/licenses/by/4.0/>).

Keywords: environmental geotechnical engineering; metro; tunnel wall; vibration response; uncertainty; accuracy

1. Introduction

The urban rail transit system, characterised by convenience and speed, has become one of the main ways of transportation for daily travel. However, the operation of an urban rail transit system may increase the environmental vibration level around the lines, bringing some adverse effects to workplaces and living environments [1–3].

To mitigate the environmental vibration problems caused by an urban rail transit system, researchers generally provide certainty ground-borne vibration prediction results through empirical methods, analytical methods, and numerical methods. Empirical methods, which usually establish empirical formulas for fast prediction, tend to be highly efficient and are preferred [4,5]. Analytical methods are based on the pipe-in-pipe model [6], the transfer matrix method [7], the semi-analytical method [8] or others for modelling soil–tunnel coupling in elastic semi-infinite space or full space, which have good computational efficiency. Numerical methods include the finite element model [9], the 2.5-dimensional finite element model [10], the finite element–infinite element model [11] and the boundary element model [12], which allow for more detailed modelling. In some cases, symmetry is used to reduce the model size and then improve computational efficiency. However, noise and vibration reduction designs based on the above methods often cannot achieve the

desired effect in actual engineering. This may lead to public complaints and even violations of regulations related to environmental vibration, resulting in adverse social impacts [13].

After extensive measures and analysis [14–16], researchers have focused on the significant uncertainty of environmental vibrations caused by an urban rail transit system. The large differences in the vibration response induced by the trains at the same position lead to an effect of uncertainty that cannot be ignored. Therefore, researchers have recently carried out many studies, using a large number of experimental methods to analyse the uncertainty associated with the vibration source intensity [17,18], the finite element method to analyse the effect of uncertainty generated by the fastening system's properties on the wheel–rail force [19], and the stochastic field theory to analyse the uncertainty of the soil propagation system [20]. At the same time, machine learning methods have been used to analyse the characteristics and sources of uncertainty in the environmental vibrations induced by the metro [21,22]. In this, the uncertainty of the intensity of vibration sources plays an important role [23]. The excitation of the vibration source subsystem can be divided into quasi-static excitation and dynamic excitation [24,25], so its uncertainty mainly comes from the differences in vehicle conditions and rail conditions [26].

Specifically, the vehicle conditions, including its axle load, wheel out-of-roundness, and maintenance level, affect the generation of vibration source strength uncertainty. Even without considering the deterioration of track conditions caused by increased operating mileage, the uncertainty caused by different vehicle conditions and loads in the short term is quite significant [27,28]. Researchers have found that differences in vibration source intensity can be caused by changes in a train's speed and axle load [29]. In addition, there is a certain difference in wheel out-of-roundness between different vehicles [30]. For example, there are corrugation excitations in the wheelset and track system, whose different wavelengths affect the frequency of wheel–rail dynamic action as well as the amplitude of the wheel–rail force [31]; the wheelsets are also operated with varying degrees of polygonality, which has a significant effect on wheel–rail system interactions [32]; and the tread surface of wheelsets tends to be flat, which generates a series of impact loads due to collisions with the rail during its movement [33]. These are crucial factors causing uncertainty in vibration source strength, and the vibration intensity strength caused by corrective wheel maintenance will be significantly reduced [34].

Rail conditions mainly refer to the unevenness of the track. There are a large number of non-periodic local defects on the rail surface, and these irregular local defects can result in significant differences in the amplitude and frequency of vibration source intensity [35]. Therefore, track unevenness can be regarded as a random process and has an impact on vibration response prediction results [36–38]. At the same time, the effects of the irregularity of short wavelength and the irregularity of medium wavelength on different frequency vibration source intensities on different track forms are different, leading to uncertainty [39].

In recent years, research on train-induced vibration considering uncertainty has been a hot topic, but most studies on train loads are based on analytical or numerical methods. However, for both vehicles and rails, their randomness is reflected in the differences in real rail vibration responses. Considering that rail vibration is easy to measure continuously in large quantities, a convenient way to quantify uncertainty is based on measured rail vibration responses. Specifically, different wheel–rail forces are obtained by inputting multiple sets of measured results into the identification method, and then the uncertainty of wheel–rail forces or train loads acting on the tunnel structure is quantified reasonably to obtain random train loads. This can provide input excitations for calculating uncertain tunnel wall (or ground) vibration responses in the probability system.

This paper aims to quantify the uncertainty of train loads and establish a symmetric numerical model for calculating the vibration response of tunnel walls in a probabilistic framework. Firstly, the wheel–rail forces and the train loads, namely the forces acting on the roadbed by the vehicle–rail system, are identified based on the measured rail vibration response. Then, the uncertainties of train loads under different speeds are quantified, which can generate a large number of random excitation loads. After that, an axisymmetric

finite element model is established, and random excitation loads are input to obtain the vibration response in the probabilistic prediction system. Finally, a prediction accuracy evaluation index that considers bias and uncertainty is used to quantify the accuracy of the prediction results.

2. Train Loads and Uncertainty Qualification

As the inputting excitation for numerical models, train loads are the bases in calculating vibration responses. The obtaining method of train loads and the uncertainty qualification method of train loads are introduced here.

Traditional methods for obtaining train loads mainly include establishing vehicle–track analytical or numerical models. Due to simplifications and assumptions in the models, some differences exist between the train loads calculated using these models and the actual situation. The measured rail accelerations can reflect the dynamic characteristics of the vehicle–track system and provide a new idea for identifying the train loads. Li et al. [40] proposed an efficient train load identification method based on an analytical model and measured rail accelerations. On this basis, a method to quantify the uncertainty of train loads based on complex principal component analysis (CPCA) and orthogonal transformation was proposed as well [41]. Therefore, the obtaining procedure of train loads considering uncertainty involves two steps: to obtain the train loads based on measurements and to quantify the uncertainty of train loads. The brief process can be seen in Figure 1.

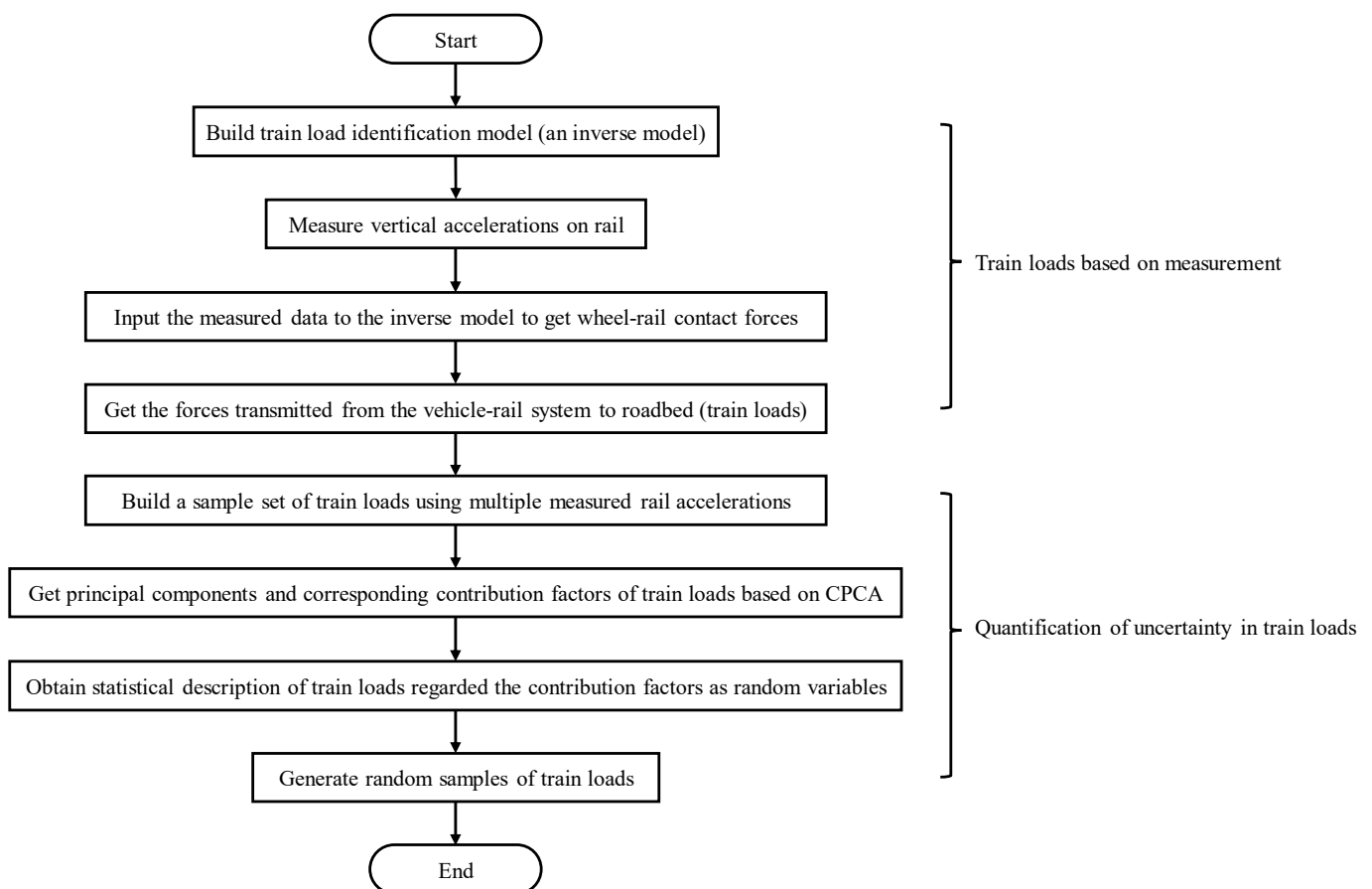


Figure 1. The process of obtaining the train loads and quantifying the uncertainties.

The first part was to retrieve the train loads based on measurements. An analytical model to identify the train loads by measured rail accelerations was established firstly. The core ideas of this model were to establish a transfer matrix of wheel–rail forces and rail

vibration responses in the frequency domain and to obtain the wheel–rail forces by solving a set of linear equations. Then, rail accelerations were measured as the inputting data of this inverse model to obtain the wheel–rail contact forces. Considering the symmetry of the vehicle–track dynamic system, the measured data for a single rail was used. According to the needs of environmental vibration research, the final step was to calculate the excitation forces transmitted from the vehicle–track system to the roadbed, i.e., the train loads for the vibration propagation models.

The second part was to quantify the uncertainty in train loads. A train loads sample set could be built using multiple measured rail accelerations induced by passages of different trains. The next step was to transform the train loads to the frequency domain through the Fourier transform. We considered the value of the train loads at each frequency as a complex random variable, so that the train loads could be viewed as a complex random vector. Via the CPCA procedure, the principal components and the corresponding contribution factors could be obtained. The principal components were regarded as the inherent features of the train loads, while the contribution factor were regarded as the contribution of each feature in the train loads. The contribution factors were random variables and their probabilistic distributions could be obtained from train load samples. Therefore, the uncertainty of train loads could be described by the uncertainty of the contribution factors. After obtaining the statistical description of the train loads uncertainty, a large number of train load samples was obtained by generating random numbers finally. This provided a basis for using the Monte Carlo method, i.e., the random simulation method, to simulate the calculation of train-induced vibrations.

3. Description of Vibration Response Uncertainty

The vibration response signals have different forms in the time domain and in the frequency domain, which require different representation methods to describe uncertainty based on their signal characteristics.

In environmental vibration research, the vibration source intensity refers to the maximum Z vibration level caused by the running trains. For underground lines, the measurement location is at the tunnel wall farthest from the other tunnel in a single-line tunnel, and the height is required to be about 1.25 m higher than the rail level. The original data for calculating the vibration source intensity are the time domain signals recorded by the sensors when the train passes. Due to differences in the vehicle conditions and axle loads of trains passing through the same section, the measured time domain signals and the one-third octave spectrum reflecting the frequency domain properties also have uncertainty. This can also result in the uncertainty of the maximum Z vibration level. To obtain a source strength considering uncertainty, it is first necessary to describe the method of describing vibration uncertainty within the probability system.

Physical quantities describing vibration responses include displacement, velocity, and acceleration. As with certainty results, results within the probability system also need to be analysed in both the time and frequency domains to evaluate the vibration response levels. In the certainty system, the amplitude of the vibration response at any given moment in the time domain is constant. In the probabilistic system, however, the amplitude of the vibration at any given moment can be described by a random variable. Meanwhile, one-third octave spectra with uncertainty can be used for description in the frequency domain. At this point, the vibration level corresponding to each centre frequency is a random variable. The Z vibration level can be obtained for each sample by weighting the vertical one-third octave spectrum, making the maximum Z vibration level a random variable.

For a certain period, the vibration response, such as the vibration acceleration $Y(t)$ at a point on the ground caused by the train running from point A to point B, can be considered using a zero-mean Gaussian process. Each calculated time history is an implementation of this Gaussian process. For each moment t_i , the vibration response $y(t_i)$ is uncertain and can

be considered a random variable, denoted as $Y(t_i)$. All random variables $Y(t_i)$ constitute a random process $Y(t)$:

$$Y(t) = \{Y(t_1), Y(t_2), Y(t_3), \dots, Y(t_n)\}. \quad (1)$$

Since the average value of the vibration response amplitude is 0, its absolute value's randomness reflects the vibration response's uncertainty. Referring to the idea of Lombaert et al. [23], the random characteristics of $|Y(t)|$ are quantified from the perspective of the ensemble average. For a Gaussian process, the square value $Y^2(t)$ of the vibration response Y at any time t , after variance normalisation, follows a chi-square distribution with 1 degree of freedom:

$$\frac{Y^2}{E(Y^2)} \sim \chi^2(1), \quad (2)$$

where $E[Y^2(t)]$ represents the mean square value of the random variable. For the vibration response at any moment, the prediction result considering uncertainty can be expressed by a confidence interval. At this time, the vibration response at the moment is an interval rather than a certainty value. The calculation of this interval requires the use of the distribution function of the chi-square distribution (Figure 2). For example, the 70% confidence interval for the response amplitude at any given moment corresponds to the 15% and 85% quantiles of the distribution function, which means the instantaneous mean square value $E[Y^2(t)]$ of $\alpha = 0.04$ times and $\beta = 2.07$ times. Therefore, the boundaries of the 70% confidence interval of the absolute value $|Y(t)|$ of the vibration response at any given moment are $\sqrt{\alpha} = 0.2$ times and $\sqrt{\beta} = 1.44$ times the instantaneous root mean square value $\text{RMS}(t_i)$. It should be noted that the instantaneous root mean square value here refers to the ensemble average obtained through statistics between different time histories at a specific moment rather than the time domain average of the same time history.

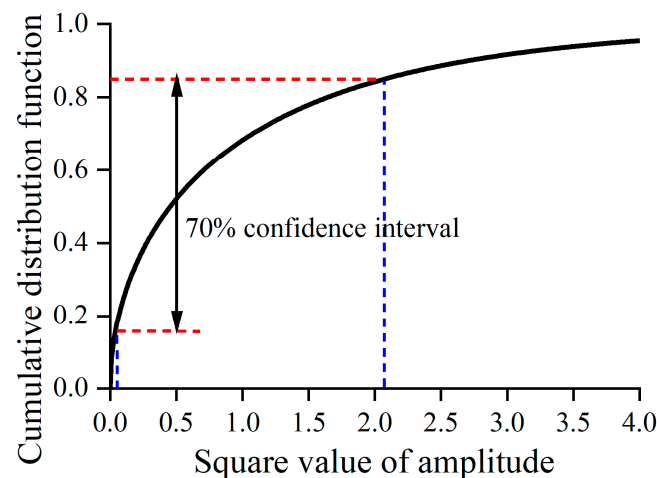


Figure 2. Cumulative distribution function of chi-squared distribution.

When considering uncertainty, both one-third octave band levels and Z vibration levels need to be represented by random variables. Each waveform curve can be processed for multiple groups of time domain signals to obtain its respective one-third octave spectrum. The probability distribution type, mean value, variance, and other statistical indicators of the one-third octave band level can be obtained by conducting statistical analysis and goodness-of-fit tests on the data set consisting of the vibration levels of each centre frequency. Similarly, the commonly used Z vibration level can be calculated by weighting the one-third octave spectra of each waveform curve. The probability distribution of the Z vibration level can be obtained by conducting statistical analysis on this set of Z vibration level data.

4. Calculation of Tunnel Wall Vibration Responses

According to the method introduced in Section 2, the train loads considering uncertainty can be obtained, and the vibration response of the tunnel or soil can be calculated by inputting it into the vibration propagation model. This section carried out measurements and calculations inside a tunnel to calculate the tunnel wall vibration responses considering uncertainty.

4.1. Project Outline

A section of the Beijing metro was selected as the research site. In this section, a double-line shield tunnel was designed with a diameter of approximately 6 m, a lining thickness of 0.3 m, and a buried depth of about 14.5 m. The rails used in this section were T60 rails. A concrete roadbed with DTVI₂-type fasteners was designed in this section. The B-type vehicles with six carriages passed through the measured cross-section. The surrounding strata of the tunnel were simplified into three layers from top to bottom: 6.2 m thick silt, 5.7 m thick fine sand, and a pebble layer. The tunnel was embedded in the pebble layer.

The acceleration measurement was conducted on the rail and tunnel wall (Figure 3). At these two points, only the vertical accelerations were measured. The acceleration sensor of the rail was installed at the bottom of the rail. Its sensitivity was 25 mv/g with a range of 200 g. The acceleration sensor of the tunnel wall was installed on the lining, which was 1.25 m away from the rail head following the Chinese standard “Technical guidelines for environmental impact assessment—Urban rail transit”. Its sensitivity was 1000 mv/g with a range of 5 g. The sampling frequencies on the two points were both set as 2048. Over 200 acceleration signals on each measured point were obtained within one day.

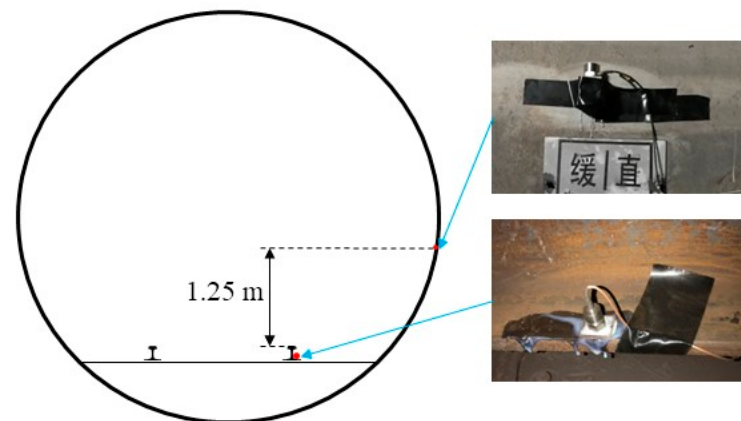


Figure 3. The measurement of accelerations on rail and tunnel wall.

4.2. Train Loads Considering Uncertainty

According to the identification of vertical wheel–rail force, multiple train loads can be obtained by inputting multiple measured vertical accelerations of the rail. Then, based on the train loads uncertainty quantification method proposed in this paper, a sufficiently large sample of train loads can be obtained. Based on this, the vertical vibration acceleration of the tunnel wall can be calculated and compared with the measurement. A total of three working conditions were selected for calculation, where the train speeds were 35 km/h, 45 km/h, and 55 km/h, respectively, with all other conditions remaining the same. The sample size of each group of vibration acceleration was set to 50, representing the overall level of vibration response in that working condition, with a representative time history of these shown in Figure 4. Considering that vibration rather than noise was the main focus, a low-pass filtering with a cutoff frequency of 200 Hz was implemented.

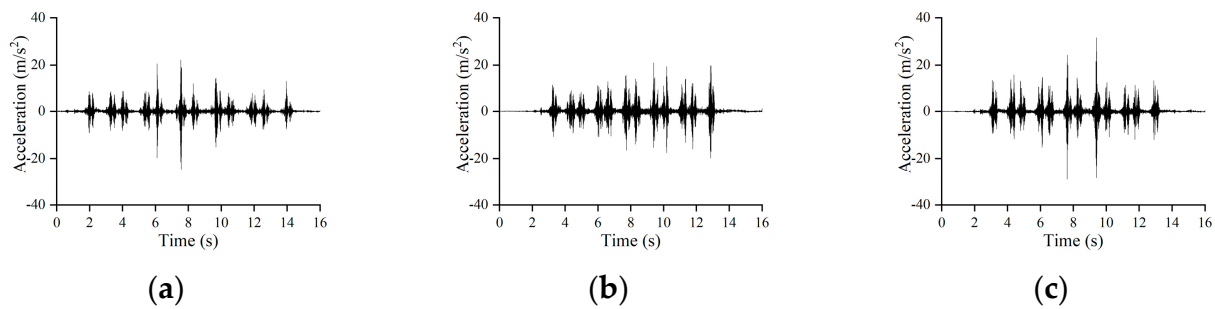


Figure 4. The measured vertical rail accelerations of the different speeds: (a) 35 km/h, (b) 45 km/h, (c) 55 km/h.

From Figure 4, it can be observed that the three-time histories show similar characteristics within a time window of 16 s, reflecting the process of the train passing through the measurement section. Comparing the three working conditions, it can be seen that as the speed of the train increases, the amplitude of the acceleration tends to increase. In response to the need for studying train-induced environmental vibration and secondary noise, the main frequency range of this study was 1~200 Hz. The sampling rate of the vibration acceleration was set at 2048, and the analysis frequency covered the study scope of both environmental vibration and secondary noise.

For each working condition, the measured time history of the vertical acceleration of the rail was successively input into the identification method [40], and 50 train loads were obtained. The rail parameters used in the identification method are shown in Table 1. The train loads here refer to the excitation forces applied on the roadbed in the 2D finite element model, which are averaged. Based on the train loads uncertainty quantification method proposed in this paper, 49 principal components and their corresponding contribution factors of the force in the frequency domain can be obtained. The principal component refers to the unit vector in the direction of the orthogonal space, which has components at any frequency. This unit vector is represented by the direction cosine of all frequencies. The contribution factor refers to the probability distribution of this principal component, described by the joint probability density function. The two-dimensional normal distribution probability density function can be visually represented by equi-probability curves. Figure 5 shows the first principal components and corresponding contribution factors of the random train loads in various working conditions. It can be seen that the first principal component has larger values within the ranges of 0~5 Hz and 50~100 Hz, corresponding to the two main peaks of the load. Assuming that all the contribution factors satisfy the complex normal distribution, each complex random variable can be described by the two-dimensional joint probability density function of the real and imaginary variables. It can be noticed that the contribution factors of each working condition have no apparent commonality, and the real and imaginary parts show a positive or negative correlation.

Table 1. The rail parameters.

Parameter	Value
Mass of rail per unit length m	60.64 kg·m ⁻¹
Moment of inertia of rail I_r	3217 cm ⁴
Elastic modulus E_r	210 GPa
Damping ratio of rail η_r	0.01
Fastener spacing L	0.6 m
Stiffness of fastener k	42 M·Nm ⁻¹
Damping of fastener c	75 kN·s·m ⁻¹

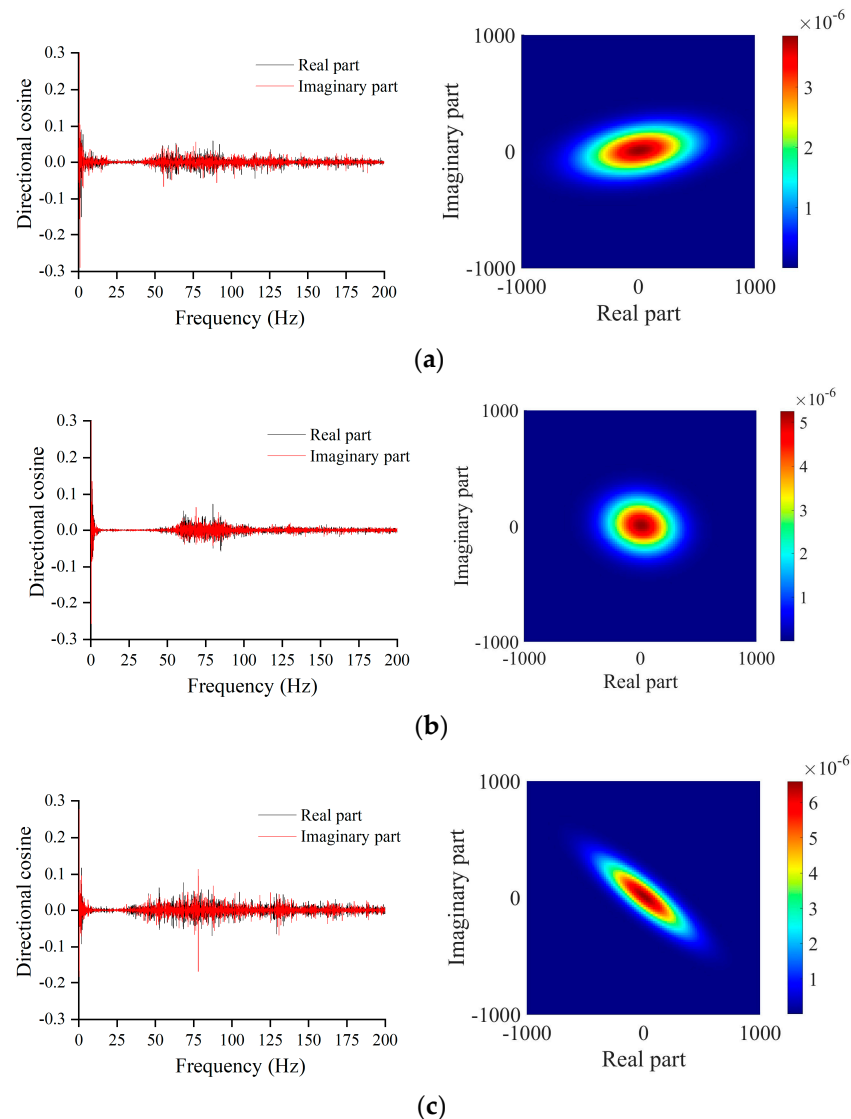


Figure 5. The first principal component and its contribution factor for different speeds: (a) 35 km/h, (b) 45 km/h, (c) 55 km/h.

Each principal component corresponds to a contribution factor in the form of a complex random variable, representing the size of the fluctuation of the random train loads in the direction of the principal component. In these three working conditions, statistics of the contribution factors corresponding to the first ten principal components of the random train loads are shown in Table 2, including the standard deviations of the real and imaginary variables and the correlation coefficient between the two. Since the train loads are initially centred, the mean value of each contribution factor is $\mu_r = 0, \mu_i = 0$. According to the sorting rule, the amplitude of the contribution factors gradually decreases, which means the fluctuation range of the train load vector in each principal component direction gradually decreases. The correlation coefficient ρ_{ri} of the different working conditions shows no obvious pattern. Taking working condition one as an example, for the first contribution factor, the real and imaginary variables are statistically positively correlated. While the two variables of the third contribution factor show a negative correlation, the two variables of the eighth contribution factor can be considered statistically uncorrelated.

Once the values of the contribution factors are determined, the random train loads in the principal component space can be transformed into the frequency domain, representing the spectrum of the train loads. Then, through the inverse Fourier transform, the time history of the train loads can be obtained. In response to the subsequent random simulation

requirements, by generating random numbers that satisfy the probability distribution of the contribution factors, a large-capacity sample of train load spectra and time history data can be generated. In this prediction, the sample size of the train loads was set at 500. Three approximately symmetrical train loads in the time domain and spectrums for each working condition are shown in Figure 6. The characteristic peaks with intervals identical to bogies can be seen.

Table 2. The statistics parameters of contribution factors for the first working condition.

Working Condition	Contribution Factor	1	2	3	4	5	6	7	8	9	10
First	σ_r	314	284	42	153	75	134	107	136	103	137
	σ_i	138	147	256	133	181	133	147	118	140	100
	ρ_{ri}	0.29	0.33	-0.61	0.60	0.32	0.17	-0.30	-0.08	0.04	0.50
Second	σ_r	196	142	73	95	90	125	104	121	104	89
	σ_i	155	109	157	141	137	98	113	92	109	117
	ρ_{ri}	-0.11	0.55	-0.09	-0.11	0.48	0.21	0.16	-0.09	-0.07	-0.33
Third	σ_r	240	148	248	236	194	153	154	167	140	124
	σ_i	201	244	121	116	157	160	150	128	149	156
	ρ_{ri}	-0.87	0.51	-0.37	-0.32	-0.62	-0.41	0.18	0.30	-0.17	0.17

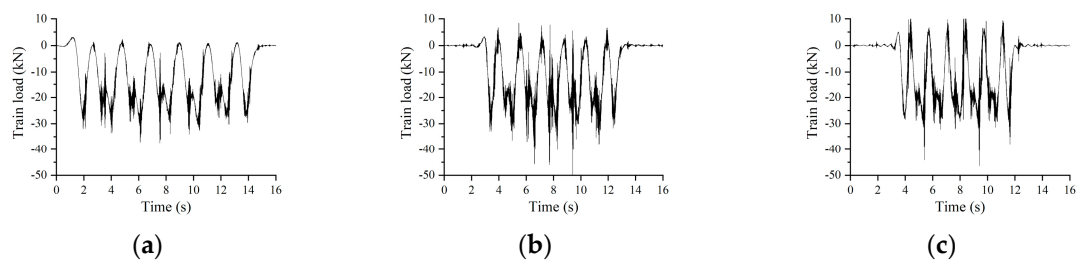


Figure 6. The samples of train loads for different speeds: (a) 35 km/h, (b) 45 km/h, (c) 55 km/h.

If the train loads are used for a 2D finite element model, it is necessary to average the train loads to obtain the equivalent loads. According to the suggestion of Xu et al. [42], an averaging process within the length range of one carriage (32 fasteners) in the time domain was carried out. The time history and frequency spectra of the processed train load are shown in Figure 7. According to the calculation requirements, the sampling rates of the train load time history in each working condition are set at 512, meeting the requirements for the analysis frequency. The waveforms and spectra show that the generated train load has similar characteristics to the original train load.

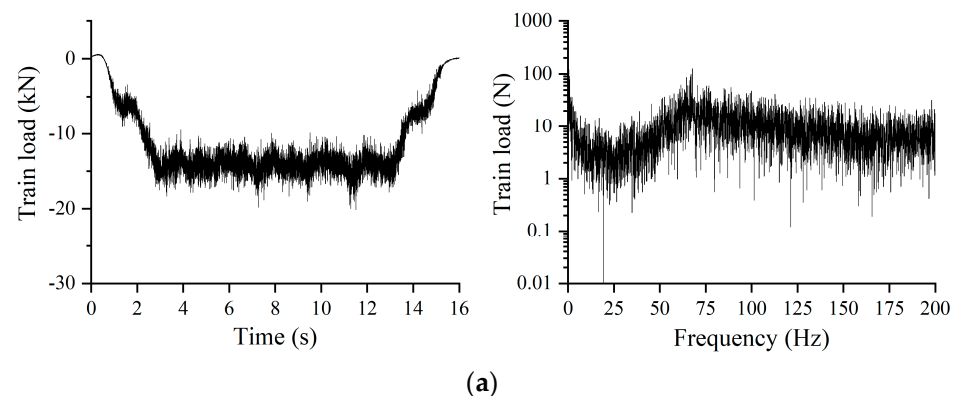


Figure 7. Cont.

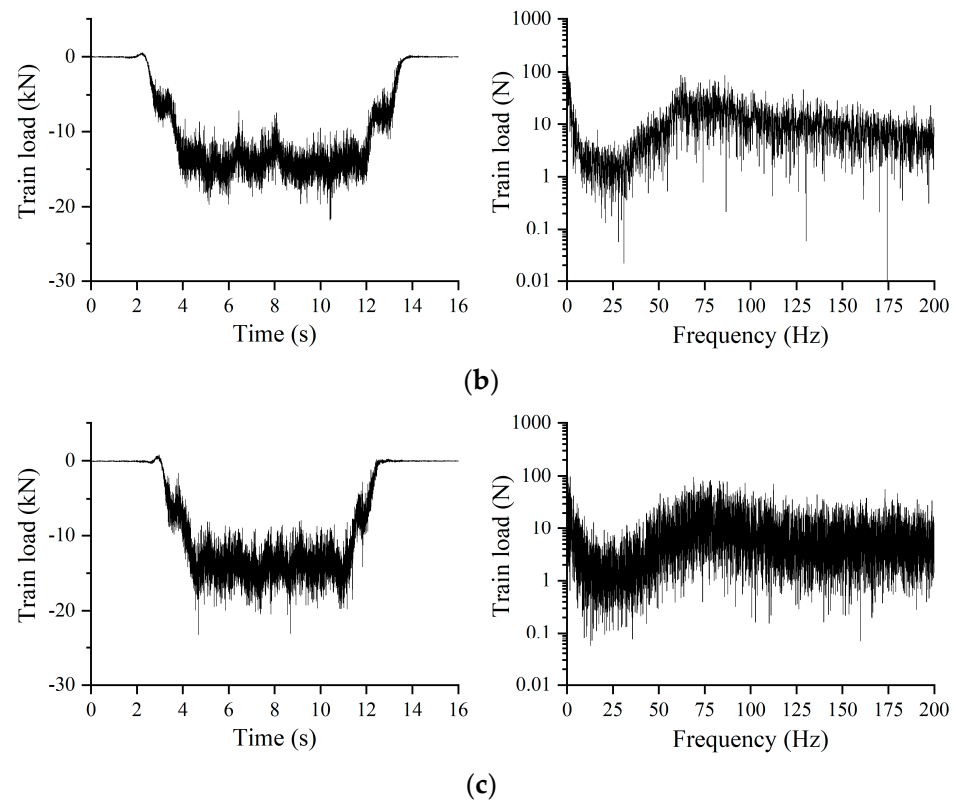


Figure 7. The train loads after averaging process in the time domain and in the frequency domain for different speeds: (a) 35 km/h, (b) 45 km/h, (c) 55 km/h.

4.3. Numerical Model

To calculate the vertical vibration response of the tunnel wall, a 2D axisymmetric finite element model shown in Figure 8 was established using ANSYS. The model was 64 m long and 50 m high, and an eight-node element was used for computation. In this case, the tunnel was embedded in a layer of pebble, with a shear wave speed of 360 m/s for the soil layer. This calculation's frequency band of interest was 1~200 Hz, resulting in a minimum shear wavelength of 1.8 m. To ensure adequate accuracy for high-frequency vibrations, the size of the soil elements surrounding the tunnel was controlled within 0.4 m so that at least four elements were included in each shear wavelength range. As the distance from the vibration source increased, the element size gradually increased to control the number of elements. The roadbed elements, tunnel elements and soil elements met the compatibility condition. A consistent viscous-spring artificial boundary was used for the model boundary, which can effectively reduce the reflection effect of waves at the boundary. Damping was modelled using the Rayleigh damping, with parameters $\alpha = 3.425$ and $\beta = 8.68 \times 10^{-5}$. For detailed descriptions of boundary and damping, refer to Ma et al. [43]. The physical and mechanical parameters of each set of elements are shown in Table 3. It was assumed that the two rails receive the same train load, which represents the fixed excitation force transmitted to the roadbed through fasteners. The input load was detailed in Section 4.2. For the calculation, we adopted transient analysis and utilized the Newmark- β method. Considering the symmetry of the model and loads, a receiver point on one side of the tunnel wall was placed at a height of 1.25 m from the rail, and the vertical acceleration of this point was recorded during the calculation process.

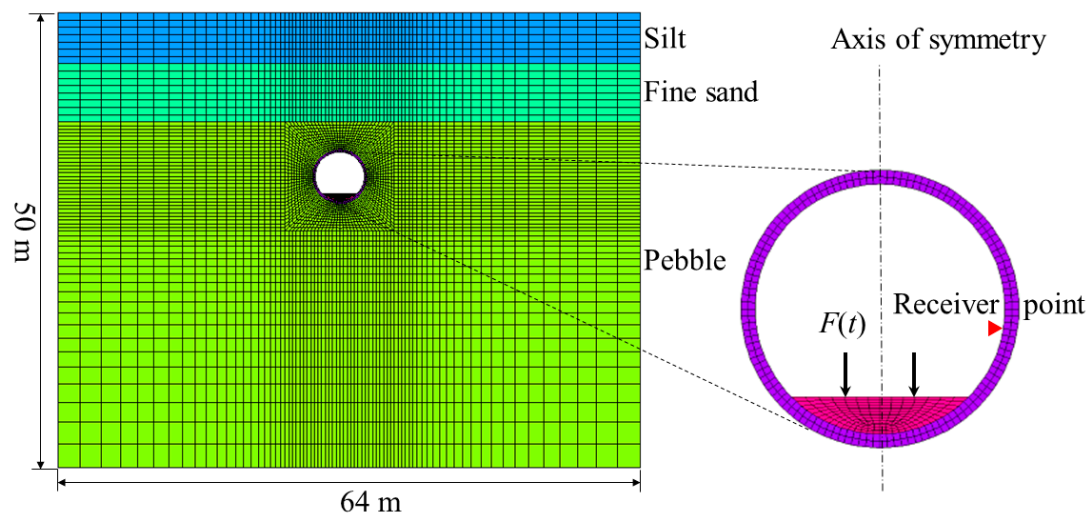


Figure 8. The numerical tunnel–soil model.

Table 3. The physical and mechanical parameters of elements.

Soil or Tunnel Structure	Density (kg/m ³)	Poisson Ratio	Elastic Modulus (MPa)	S-Wave Speed (m/s)	P-Wave Speed (m/s)	Damping Ratio
Lining	2500	0.2	30,000	-	-	0.03
Roadbed	2500	0.2	28,000	-	-	0.03
Silt	1940	0.3	113	150	260	0.03
Fine sand	2030	0.3	248	220	370	0.03
Pebble	2150	0.3	720	360	650	0.03

Since the purpose of this research was to quantify the uncertainty of the vibration source intensity, the Monte Carlo method was adopted for the calculation. In this method, the probability prediction was decomposed into several certainty calculations, and each calculation process did not interact. By successively applying a single train load to the numerical model, 500 vibration responses could be calculated, and then statistical analysis could be performed to obtain the statistical rules of the receiver point response.

4.4. Analysis of Results

Once the vertical vibration acceleration sample set of the receiver point on the tunnel wall was obtained, the random characteristics of the vibration response could be described using the uncertainty quantification methods in the time domain and frequency domain presented in this paper. In the time domain, the uncertainty was described using the instantaneous root mean square values of the vibration amplitudes under ensemble averaging. In each working condition, there was a 90% confidence interval of the instantaneous root mean square of the vertical acceleration of the tunnel wall, as shown in Figure 9. It can be seen that the confidence interval range of the predicted results and the measured results was very close. With an increase in train speed, both the upper limits of the predicted and measured confidence intervals showed an increasing trend. The measured results can reflect the characteristics of different axle passages through the measurement section. However, since the train load in the prediction model was subjected to averaging treatment, the passing effect of different axles was not evident.

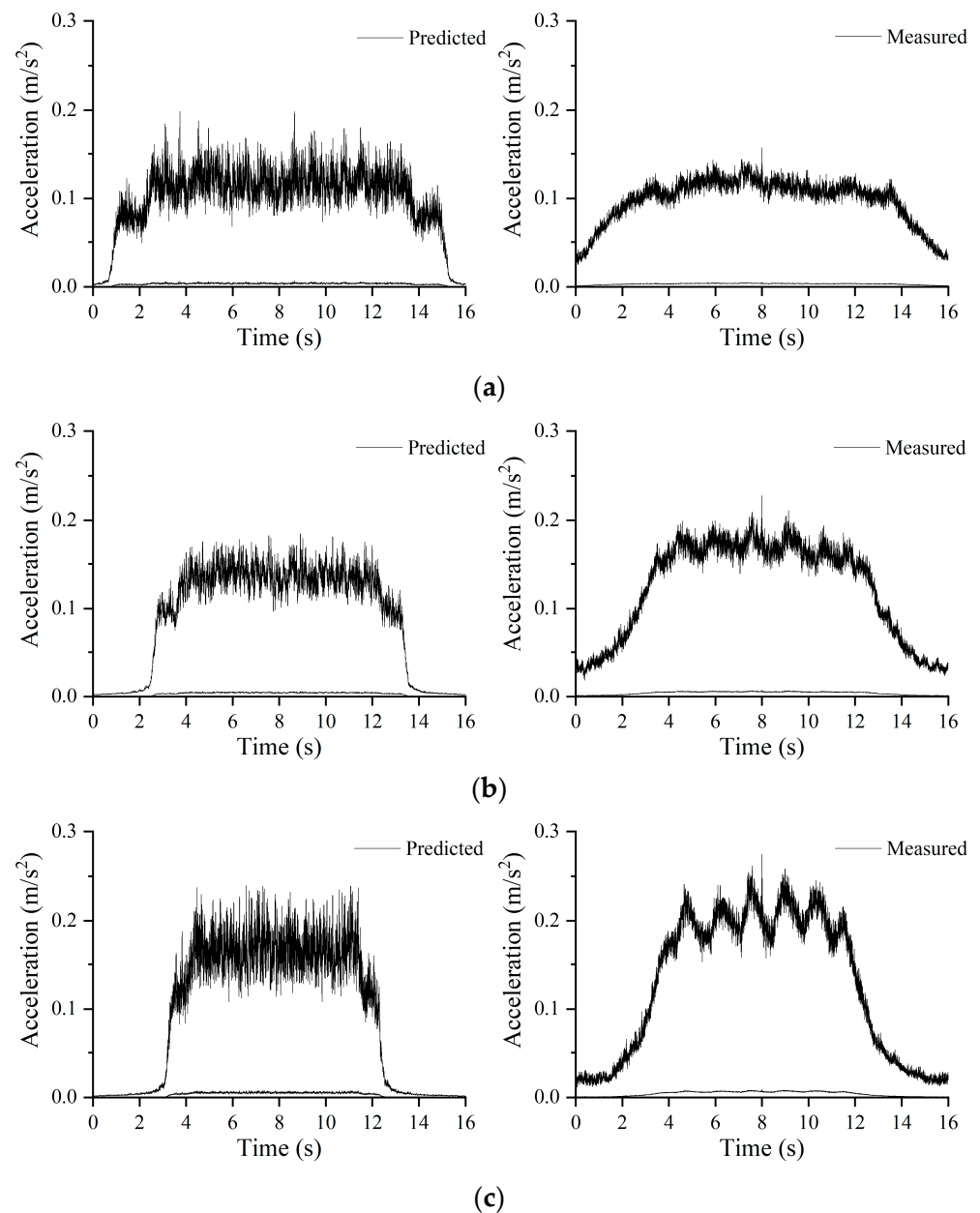


Figure 9. The 90% confidence interval of instantaneous RMS of vertical accelerations on the tunnel wall: (a) 35 km/h, (b) 45 km/h, (c) 55 km/h.

A one-third octave spectrum analysis was performed on each predicted and measured time history. Then, the vibration level corresponding to each centre frequency was treated as a continuous random variable, and the probability distribution of the vibration level at specific frequencies could be obtained through statistical analysis. After obtaining statistical parameters such as the mean and standard deviation, the confidence intervals at a certain confidence level could be obtained. As shown in Figure 10, the black lines represent the average one-third octave vibration levels of the predicted and measured results, and the grey bands represent the 90% confidence interval of the one-third octave vibration levels. It can be seen that the average predicted and measured values have the same trend with the change of frequency, and the vibration levels corresponding to each centre frequency are relatively close. In terms of uncertainty, the width of the 90% confidence interval of the vibration level at each frequency is also quite close.

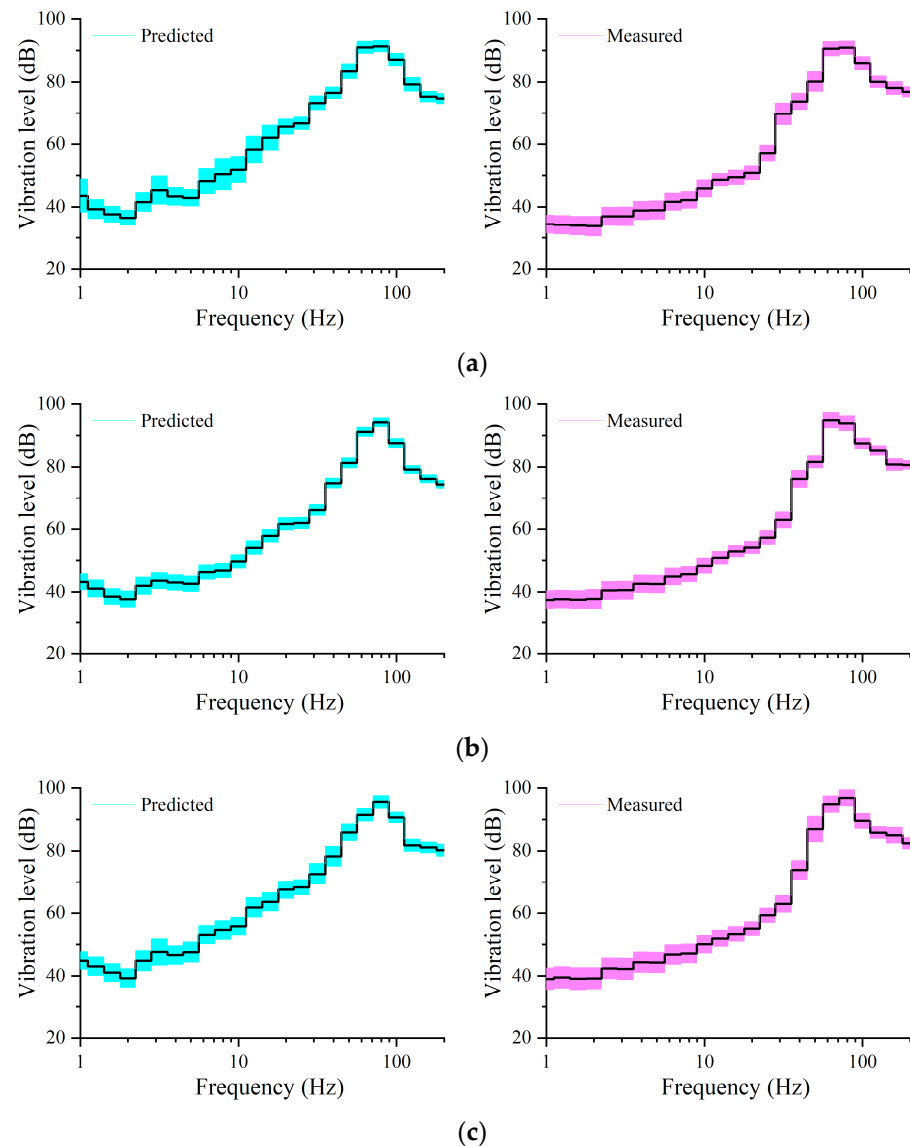


Figure 10. The 90% confidence interval of the one-third octave bands of vertical accelerations on the tunnel wall: (a) 35 km/h, (b) 45 km/h, (c) 55 km/h.

The calculation results of the tunnel wall vibration response are evaluated using the prediction accuracy evaluation method [41]. The predictions considering uncertainty and the measured results are denoted as random variables X_p and X_m , respectively. The distribution of the two-dimensional random vector (X_p, X_m) on the plane can reflect the accuracy of the predicted results. The closer the two-dimensional random vector is to the $y = x$, the more accurate the prediction result. The root mean square error of the two random variables X_p and X_m is given as the following:

$$\text{RMSE} = \sqrt{\int_{-\infty}^{+\infty} \int_{-\infty}^{+\infty} h(x_p, x_m) (x_p - x_m)^2 dx_m x_p}, \quad (3)$$

where $h(x_p, x_m)$ represents the probability density function of the two-dimensional random vector (X_p, X_m) . For descriptive convenience, the relative value after normalisation is used to define the accuracy of the prediction results:

$$\text{PAI} = 1 - \frac{\text{RMSE}}{\mu_m}, \quad (4)$$

where μ_m represents the mathematical expectation of the measured random variable X_m . It can be seen that PAI is a dimensionless quantity, and the larger its value, the more accurate the prediction.

Assuming that the vibration levels at each centre frequency are normally distributed, and assuming that the correlation coefficient between the predicted and measured values is 0.8 based on prior information, the PAI values of the one-third octave vibration level in each working condition can be calculated, as shown in Figure 11. It can be seen that the PAI values reach 0.65 or above at each centre frequency, which overall shows a high level of accuracy for the predicted values. In these three working conditions, the PAI values show a similar trend with frequency, maintaining a relatively high level below 4 Hz and above 40 Hz. The least accurate prediction is at the centre frequency of 20 Hz, where the bias between the predicted and measured results is larger.

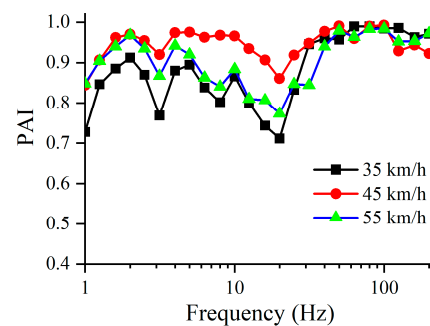


Figure 11. The PAI values of the one-third octave bands of vertical accelerations on the tunnel wall.

Based on the same principle and process, the maximum Z vibration level can also be treated as a continuous random variable, and its probability distribution can be obtained. In each prediction case, by performing a maximum Z vibration level analysis on each acceleration time history of the predicted results, a sample of the maximum Z vibration level with a sample size of 500 can be obtained. As shown in Figure 12, this sample can be presented in the form of a frequency distribution histogram. By conducting a K-S test with a significance level of $\alpha = 0.05$ on the maximum Z vibration level samples in these three working conditions, it can be found that all follow a normal distribution. According to the distribution of the samples, a continuous probability density function curve can be fitted, and the vertical axis of this curve has the same coordinate scale as the frequency density. From the perspective of mean values, the predicted values in all three working conditions are close to the measured values, with biases of 0.19 dB, -2.94 dB, and -2.64 dB, respectively. From the perspective of standard deviation, the standard deviations of the predicted values in cases 1 and 2 are smaller than those of the measured values; in the last working condition, the standard deviations of the predicted and measured values are very close.

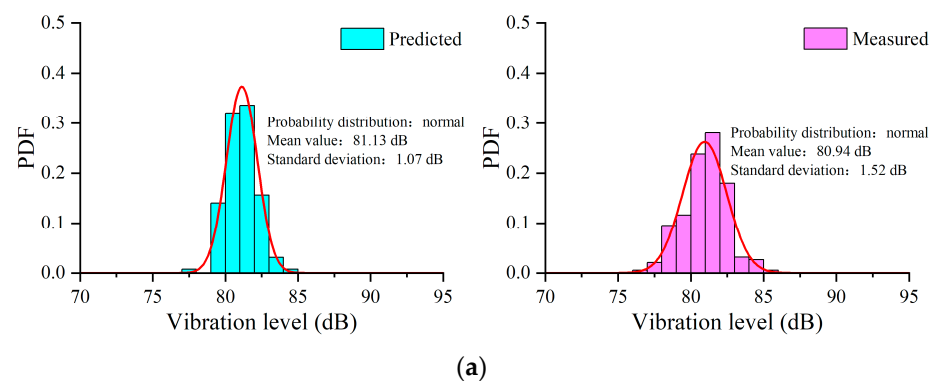


Figure 12. Cont.

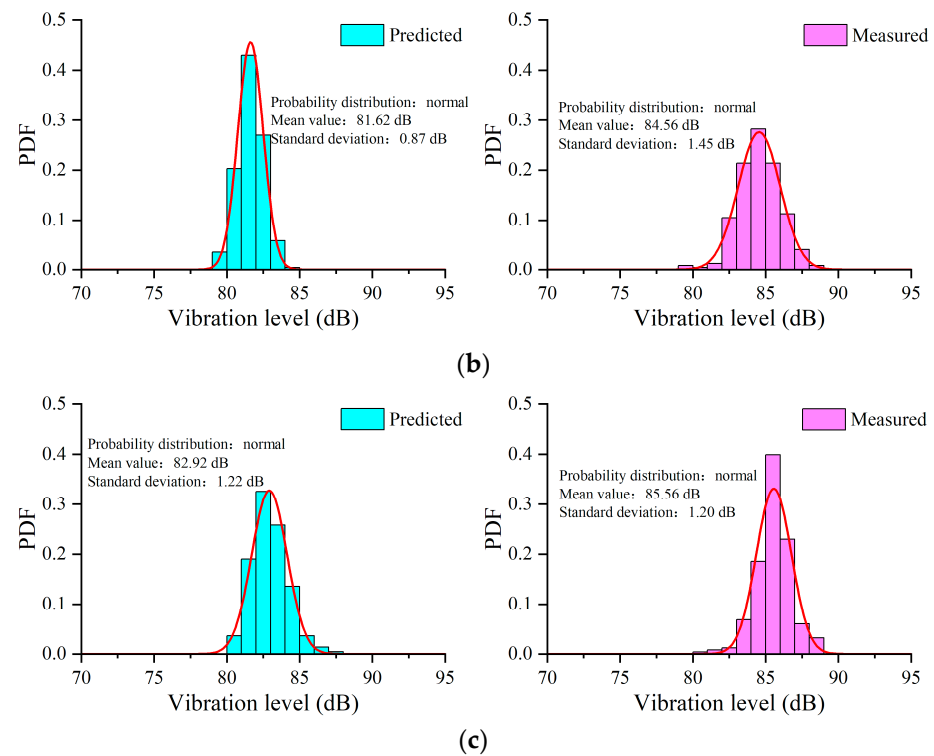


Figure 12. The probabilistic distribution histograms and fitting curves (red lines) of the maximum Z vibration levels of vertical accelerations on the tunnel wall: (a) 35 km/h, (b) 45 km/h, (c) 55 km/h.

To visually represent this, the joint probability density function of the predicted and measured values are displayed in Figure 13. The equal probability ellipses for all three working conditions are located near the reference line $x_m = x_p$, showing high accuracy. The state of the ellipse also reflects the bias and uncertainty of the prediction. For the latter two working conditions, the centre of the ellipse is in the upper left of the plane, indicating that the prediction underestimates the mean value. The first two ellipses show a “raised head” state, indicating that the predicted values underestimates the uncertainty. The accuracy index PAI is also used to evaluate the effect of the maximum Z vibration level prediction. The PAI values for these three working conditions reach 0.99, 0.96, and 0.97, respectively, showing high prediction accuracy. For the prediction of vibration source strength, the distance between the train load and the receiver point is very close, and the vibration propagation path is relatively clear. Moreover, the vibration mainly propagates in the concrete structure, so the accurate prediction of vibration source strength directly reflects the high accuracy of the random train loads.

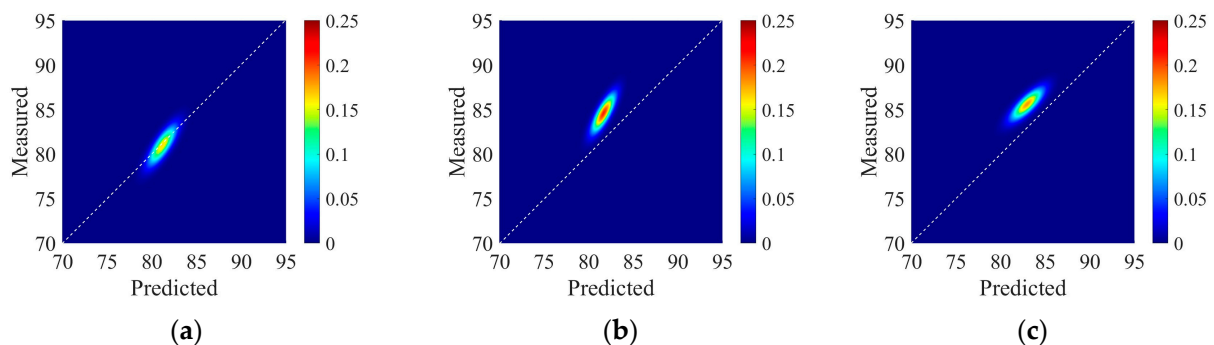


Figure 13. The joint distributions of predicted and measured maximum Z vibration levels on the tunnel wall: (a) 35 km/h, (b) 45 km/h, (c) 55 km/h.

On the other hand, the PAI values and the joint distributions of prediction and measurement show a certain degree of difference in different working conditions. The PAI value under the first working condition is the highest, indicating a good fit between the elliptical-shaped bright spot of the joint distribution and the reference line. The bright spots under the second working condition show a “rising” appearance, indicating that the predicted values underestimate uncertainty, resulting in the lowest PAI value. Under the third operating condition, the long axis of the bright spot is parallel to the reference line, indicating that the uncertainty of the predicted and measured values is consistent, but the prediction overestimates the average vibration response. This difference is not significantly related to the vehicle speed, but it is caused by the superposition of various accidental factors.

5. Conclusions

This paper quantified the uncertainty of train loads and established a symmetric numerical model for calculating the vibration response of tunnel wall in a probabilistic framework. By comparing the calculated results with the measurements, some conclusions can be drawn.

- (1) A method for quantifying the uncertainty of train loads is introduced, based on the identification method as well as the principal component analysis method to generate large-capacity samples to reflect the randomness of the loads. Then, the method to describe the uncertainty of train-induced vibrations in the time domain and frequency domain is presented.
- (2) The probabilistic distributions of the vibration response of the tunnel wall under three different train speeds are calculated using the random simulation method and compared with the measured results. The results show that the amplitude and trend of the predicted and measured results are similar, and the predicted and measured results are in good agreement in terms of bias and uncertainty.
- (3) An accuracy index PAI was used to quantitatively evaluate the calculation accuracy of the proposed method. The results show that the PAI value reaches more than 0.65 at each centre frequency, indicating that the proposed method has high accuracy and that the bias between the prediction results and the measured results is within an acceptable range. Since the vibration propagation path inside the tunnel is short, the accurate results of vibration responses directly reflect the accuracy of train loads.
- (4) The accuracies represented by PAI values under different speeds show differences, but the differences are not significantly related to the vehicle speed.
- (5) In the socio-economic sense, accurate predicted results are beneficial for selecting appropriate vibration mitigation measures during the design phase. It helps to balance the risk of excessive vibration and the risk of excessive use of vibration mitigation measures. The latter usually means higher prices.

Author Contributions: Conceptualization, C.L.; methodology, Z.W. and C.L.; software, D.L.; validation, D.L. and B.Z.; formal analysis, B.Z.; investigation, D.L.; resources, W.L. and W.W.; writing—original draft, Z.W.; writing—review and editing, C.L. and W.L.; visualization, D.L.; supervision, W.L.; project administration, W.W.; funding acquisition, Z.W. and W.L. All authors have read and agreed to the published version of the manuscript.

Funding: This research was funded by China Academy of Railway Sciences Corporation Limited, grant number 2023YJ090.

Data Availability Statement: Readers can directly contact the corresponding author to obtain the data in this article.

Acknowledgments: The authors thank the reviewers for their valuable suggestions.

Conflicts of Interest: The authors declare no conflicts of interest.

References

1. Li, X.; Chen, Y.; Zou, C.; Chen, Y. Train-induced vibration mitigation based on foundation improvement. *J. Build. Eng.* **2023**, *76*, 107106. [[CrossRef](#)]
2. Liu, X.; Xiao, Y.; Jiang, H.; Guo, Y.; Yu, M.; Tan, W. Analogical Assessment of Train-Induced Vibration and Radiated Noise in a Proposed Theater. *Sensors* **2023**, *23*, 505. [[CrossRef](#)]
3. Bharathi, M.; Raj, D.; Singh, Y. Metro Train-Induced Vibration Measurement on Buildings. In *Earthquakes and Structures: Select Proceedings of 7th ICRAGEE 2021*; Springer: Singapore, 2022; pp. 201–212.
4. Quagliata, A.; Ahearn, M.; Boeker, E.; Meister, L.; Administration, F.T. *Transit Noise and Vibration Impact Assessment Manual (FTA Report No.0123)*; U. S. Department of Transportation: Washington, DC, USA, 2018.
5. Ministry of Ecology and Environment of the People's Republic of China. *Technical Guidelines for Environmental Impact Assessment-Urban Rail Transit*; Ministry of Ecology and Environment of the People's Republic of China: Beijing, China, 2018. (In Chinese)
6. Hussein, M.; Hunt, H. A numerical model for calculating vibration from a railway tunnel embedded in a full-space. *J. Sound Vib.* **2007**, *305*, 401–431. [[CrossRef](#)]
7. Xu, L.; Ma, M. Analytical solution of ground-borne vibration due to a spatially periodic harmonic moving load in a tunnel embedded in layered soil. *J. Zhejiang Univ. Sci. A* **2023**, *24*, 637–652. [[CrossRef](#)]
8. Tao, Z.-Y.; Zou, C.; Yang, G.-R.; Wang, Y.-M. A semi-analytical method for predicting train-induced vibrations considering train-track-soil and soil-pile-building dynamic interactions. *Soil Dyn. Earthq. Eng.* **2023**, *167*, 107822. [[CrossRef](#)]
9. Ren, Y.; Qu, S.; Yang, J.; Li, Q.; Zhu, B.; Zhai, W.; Zhu, S. An efficient three-dimensional dynamic stiffness-based model for predicting subway train-induced building vibrations. *J. Build. Eng.* **2023**, *76*, 107239. [[CrossRef](#)]
10. Feng, S.; Li, Y.; Li, J. Prediction and mitigation analysis of railway-induced vibrations of a layered transversely isotropic ground comprising different media with a hybrid 2.5-D method. *Comput. Geotech.* **2023**, *159*, 105461. [[CrossRef](#)]
11. Wang, S.; Cao, Z.; Xu, Y.; Xiao, Z.; Yuan, Z.; Cai, Y.; Gou, C. Prediction and mitigation of train-induced vibrations of over-track buildings on a metro depot: Field measurement and numerical simulation. *J. Vib. Control* **2023**, *29*, 5413–5426. [[CrossRef](#)]
12. Andersen, L.; Jones, C. Coupled boundary and finite element analysis of vibration from railway tunnels—A comparison of two-and three-dimensional models. *J. Sound Vib.* **2006**, *293*, 611–625. [[CrossRef](#)]
13. Vasheghani, M.; Sadeghi, J.; Khajehdezfuly, A. Legal consequences of train-induced structure borne noise and vibration in residential buildings. *Noise Mapp.* **2022**, *9*, 170–188. [[CrossRef](#)]
14. Connolly, D.; Costa, P.A.; Kouroussis, G.; Galvin, P.; Woodward, P.; Laghrouche, O. Large scale international testing of railway ground vibrations across Europe. *Soil Dyn. Earthq. Eng.* **2015**, *71*, 1–12. [[CrossRef](#)]
15. Di, H.; Yu, J.; Guo, H.; Zhou, S.; He, C.; Zhang, X. Modeling of ground vibrations from a tunnel in layered unsaturated soil with spatial variability. *Arch. Civ. Mech. Eng.* **2022**, *22*, 33. [[CrossRef](#)]
16. Qu, X.; Thompson, D.; Ma, M.; Li, M.; Ntsios, E. Sources of variability in metro train-induced vibration. *Proc. Inst. Mech. Eng. Part F J. Rail Rapid Transit* **2023**, *237*, 490–499. [[CrossRef](#)]
17. Ma, M.; Li, M.; Qu, X.; Zhang, H. Effect of passing metro trains on uncertainty of vibration source intensity: Monitoring tests. *Measurement* **2022**, *193*, 110992. [[CrossRef](#)]
18. He, Y.; Peng, L.; He, K.; Guan, Q.; Han, J.; Xiao, X.; Sheng, X. Analysis of uncertainty and variation in underground train-induced vibration based on measured data. *Measurement* **2023**, *222*, 113600. [[CrossRef](#)]
19. Sadeghi, J.; Seyedkazemi, M.; Khajehdezfuly, A. Effect of uncertainty of fastening systems properties on wheel/rail dynamic force. *Lat. Am. J. Solids Struct.* **2021**, *18*, e381. [[CrossRef](#)]
20. Deng, E.; Liu, X.-Y.; Ni, Y.-Q.; Wang, Y.-W.; Zhao, C.-Y. A coupling analysis method of foundation soil dynamic responses induced by metro train based on PDEM and stochastic field theory. *Comput. Geotech.* **2023**, *154*, 105180. [[CrossRef](#)]
21. Liu, W.; Liang, R.; Zhang, H.; Wu, Z.; Jiang, B. Deep learning based identification and uncertainty analysis of metro train induced ground-borne vibration. *Mech. Syst. Signal Process.* **2023**, *189*, 110062. [[CrossRef](#)]
22. Liang, R.; Liu, W.; Li, C.; Li, W.; Wu, Z. A novel efficient probabilistic prediction approach for train-induced ground vibrations based on transfer learning. *J. Vib. Control* **2023**, *30*, 10775463221148792. [[CrossRef](#)]
23. Lombaert, G.; Galvín, P.; François, S.; Degrande, G. Quantification of uncertainty in the prediction of railway induced ground vibration due to the use of statistical track unevenness data. *J. Sound Vib.* **2014**, *333*, 4232–4253. [[CrossRef](#)]
24. Colaço, A.; Costa, P.A.; Connolly, D.P. The influence of train properties on railway ground vibrations. *Struct. Infrastruct. Eng.* **2016**, *12*, 517–534. [[CrossRef](#)]
25. Wang, L.; Zhu, Z.; Bai, Y.; Li, Q.; Costa, P.A.; Yu, Z. A fast random method for three-dimensional analysis of train-track-soil dynamic interaction. *Soil Dyn. Earthq. Eng.* **2018**, *115*, 252–262. [[CrossRef](#)]
26. Hunt, H.; Hussein, M. Vibration from railways: Can we achieve better than +/-10dB prediction accuracy? In Proceedings of the 14th International Congress on Sound and Vibration 2007, Cairns, Australia, 9–12 July 2007; pp. 3212–3219.
27. Kuo, K.A.; Lombaert, G.; Degrande, G. Quantifying uncertainties in measurements of railway vibration. In *Noise and Vibration Mitigation for Rail Transportation Systems*; Springer: Berlin, Germany, 2018; pp. 155–166.
28. Xu, Z.; Ma, M.; Zhou, Z.; Xie, X.; Xie, H.; Jiang, B.; Zhang, Z. Prediction of metro train-induced tunnel vibrations using machine learning method. *Adv. Civ. Eng.* **2022**, *2022*, 4031050. [[CrossRef](#)]
29. Heidary, R.; Esmaeili, M.; Gharouni Nik, M. Effects of train operational parameters on ground-borne vibrations induced by twin metro tunnels. *Int. J. Rail Transp.* **2021**, *9*, 144–156. [[CrossRef](#)]

30. Tao, G.; Liu, M.; Xie, Q.; Wen, Z. Wheel–rail dynamic interaction caused by wheel out-of-roundness and its transmission between wheelsets. *Proc. Inst. Mech. Eng. Part F J. Rail Rapid Transit* **2022**, *236*, 247–261. [[CrossRef](#)]
31. Wang, Z.; Lei, Z. Dynamic characteristics of a wheelset–track system under corrugation excitations in the metro operation process. *Trans. Can. Soc. Mech. Eng.* **2020**, *45*, 411–420. [[CrossRef](#)]
32. Yang, Y.; Ling, L.; Wang, C.; Liu, Z.; Wang, K.; Zhai, W. Wheel/rail dynamic interaction induced by polygonal wear of locomotive wheels. *Veh. Syst. Dyn.* **2022**, *60*, 211–235. [[CrossRef](#)]
33. Bogdevičius, M.; Žygienė, R.; Dailydka, S.; Bartulis, V.; Skrickij, V.; Pukalskas, S. The dynamic behaviour of a wheel flat of a railway vehicle and rail irregularities. *Transport* **2015**, *30*, 217–232. [[CrossRef](#)]
34. Nielsen, J.; Mirza, A.; Cervello, S.; Huber, P.; Müller, R.; Nelain, B.; Ruest, P. Reducing train-induced ground-borne vibration by vehicle design and maintenance. *Int. J. Rail Transp.* **2015**, *3*, 17–39. [[CrossRef](#)]
35. Kouroussis, G.; Connolly, D.P.; Alexandrou, G.; Vogiatzis, K. The effect of railway local irregularities on ground vibration. *Transp. Res. Part D Transp. Environ.* **2015**, *39*, 17–30. [[CrossRef](#)]
36. Zhu, Z.; Wang, L.; Costa, P.A.; Bai, Y.; Yu, Z. An efficient approach for prediction of subway train-induced ground vibrations considering random track unevenness. *J. Sound Vib.* **2019**, *455*, 359–379. [[CrossRef](#)]
37. Song, L.; Liu, H.; Xu, L.; Yu, Z. Random simulation method of track irregularities and its application in vehicle-track dynamic analysis. *Int. J. Rail Transp.* **2023**, *11*, 169–187. [[CrossRef](#)]
38. Xu, L.; Zhao, Y.; Zhu, Z.; Li, Z.; Liu, H.; Yu, Z. Vehicle-track random vibrations considering spatial frequency coherence of track irregularities. *Veh. Syst. Dyn.* **2022**, *60*, 3977–3998. [[CrossRef](#)]
39. Xu, Q.-Y.; Ou, X.; Au, F.; Lou, P.; Xiao, Z.-C. Effects of track irregularities on environmental vibration caused by underground railway. *Eur. J. Mech. A/Solids* **2016**, *59*, 280–293. [[CrossRef](#)]
40. Li, C.; Liu, W.; Liang, R. Identification of vertical wheel-rail forces based on an analytical model and measurement and its application in predicting ground-borne vibration. *Measurement* **2021**, *186*, 110182. [[CrossRef](#)]
41. Li, C.; Liu, W. Probabilistic prediction of metro induced ground-borne vibration and its accuracy evaluation. *Soil Dyn. Earthq. Eng.* **2021**, *141*, 106509. [[CrossRef](#)]
42. Xu, Q.; Xiao, Z.; Liu, T.; Lou, P.; Song, X. Comparison of 2D and 3D prediction models for environmental vibration induced by underground railway with two types of tracks. *Comput. Geotech.* **2015**, *68*, 169–183. [[CrossRef](#)]
43. Ma, M.; Liu, W.; Qian, C.; Deng, G.; Li, Y. Study of the train-induced vibration impact on a historic Bell Tower above two spatially overlapping metro lines. *Soil Dyn. Earthq. Eng.* **2016**, *81*, 58–74. [[CrossRef](#)]

Disclaimer/Publisher’s Note: The statements, opinions and data contained in all publications are solely those of the individual author(s) and contributor(s) and not of MDPI and/or the editor(s). MDPI and/or the editor(s) disclaim responsibility for any injury to people or property resulting from any ideas, methods, instructions or products referred to in the content.